Applied Thermal Engineering 196 (2021) 117230

Contents lists available at ScienceDirect

Applied Thermal Engineering

journal homepage: www.elsevier.com/locate/apthermeng

Integration of radiative sky cooling to the photovoltaic and thermoelectric system for improved space cooling

Trevor Hocksun Kwan, Datong Gao, Bin Zhao, Xiao Ren, Tianxiang Hu, Yousef N. Dabwan, Gang Pei *

Department of Thermal Science and Energy Engineering, University of Science and Technology of China, China

ARTICLE INFO

Keywords:
Space cooling
Hybrid cooling system
Photovoltaic panel
Radiative sky cooling
Thermoelectric cooler

ABSTRACT

The feasibility of integrating the radiative sky cooling ability of common photovoltaic cells into the photovoltaic-thermoelectric cooler to further enhance the space cooling energy density is analyzed in this paper. Specifically, daytime cooling is obtained by the photovoltaic panel powering the thermoelectric cooler while the same photovoltaic panel provides nighttime radiative sky cooling. To achieve an optimal temporal match between the new method's output cooling power to a cooling building's time-varying cooling load (with 4 occupants and 24 m^2 floor space), two thermoelectric cooler modes of operation are studied; The first continuously operates the thermoelectric cooler power at the time-averaged value while the second directly supplies the photovoltaic power to the thermoelectric cooler in the daytime. Furthermore, a spectral model is used to accurately estimate the radiative energy of crystalline solar cells based on their emissivity spectrum. It is found that radiative sky cooling can almost double the equivalent solar to cooling coefficient of performance over the basic photovoltaic and thermoelectric cooler system (from 0.1099 to 0.2054). The photovoltaic area only needed to be 12–17 m^2, and the second operating mode can better match the supply versus cooling demand ratio while yielding a relatively consistent 10 °C difference throughout the entire day.

1. Introduction

Despite being a very important aspect of everyday life to ensure the personal comfort and health of the occupants, space cooling occupies a very significant portion of the building's energy consumption (e.g., around 60% in regions near the equator such as Singapore [1]). Currently, the heat pump (HP) engine is most commonly used to satisfy the cooling demands, which uses an applied work to forcibly drive heat transfer from a low-temperature environment into a higher temperature one. HPs have already been widely implemented either as the vapor compression cycle (VCC) (i.e., The common air conditioner) [2,3] or as a thermoelectric cooler (TEC) for smaller-scale applications [4,5]. However, the applied work is most commonly being supplied by fossil fuel power plants, which is worsening environmental issues such as global warming, climate change, and air pollution. Thus, an alternative is urgently needed, and one approach is to use a renewable energy source to drive the HP.

In particular, solar energy is a clean energy source that is available almost anywhere on the Earth, but the sun is naturally a high-temperature (≈ 6000 K) blackbody radiator [6]. This means a systematic method is required to convert this into cooling energy, which is currently being achieved by either coupling solar thermal collectors to the absorption chiller (AC) [7,8], or using a photovoltaic (PV) panel to convert the sunlight into electricity for driving the HP. The latter is more attractive because it avoids the exergy losses that incur in the solar to heat conversion process. Furthermore, the HP choice affects the PV-HP system's energy performance, so many researchers have studied the vapor compression cycle (VCC) because it yields a higher coefficient of performance (COP), such as (a solar to cooling equivalent) range of 1.85–2.25 as reported by Salilih and Birhane [9]. Furthermore, Fong et al. [10] included an ejector into this system to produce chilled water at even higher energy efficiencies. Besides providing cooling energy to the end-user, another recent approach is cooling down the PV cells through the VCC while the waste heat from the hot side is harnessed for space/water heating applications. Doing so can significantly lower the PV panel temperature, thus increasing the cell lifetime and production efficiency. This idea has been studied by Lu et al. [11] and our previous

* Corresponding author.
E-mail addresses: trobby@ustc.edu.cn (T.H. Kwan), gaodt@mail.ustc.edu.cn (D. Gao), zb630@mail.ustc.edu.cn (B. Zhao), rx1008@mail.ustc.edu.cn (X. Ren), htx@mail.ustc.edu.cn (T. Hu), Dabwan@ustc.edu.cn (Y.N. Dabwan), peigang@ustc.edu.cn (G. Pei).

https://doi.org/10.1016/j.applthermaleng.2021.117230
Received 22 January 2021; Received in revised form 7 June 2021; Accepted 9 June 2021
Available online 16 June 2021

Nomenclature

Abbreviations

BB	Blackbody Radiation
COP	Coefficient of performance
CPV	Concentrated Photovoltaic
DC	Direct Current
BB	Blackbody Radiation
IR	Infrared
PV	Photovoltaic
RSC	Radiative Sky Cooling
RH	Relative Humidity
TEC	Thermoelectric Cooler
VCC	Vapor Compression Cycle

Variables

a	Ideal Diode Constant (0–1)
A_{RSC}	Radiative sky cooling surface area (m^2)
A_{wall}	The surface area of the building wall (m^2)
A_{req}	Required surface area of the PV panel (m^2)
$A_{req(T.S.)}$	Required surface area of the PV panel if thermal storage is included in the system (m^2)
α	Seebeck coefficient (W/K)
COP_{Eq}	The equivalent solar to cooling energy coefficient of performance
E_{Bat}	The required battery size (Wh)
E_T	The required thermal storage capacity (Wh)
e_{Bat}	The recorded amount of electricity within each timestep (Wh)
e_T	The recorded amount of thermal energy within each timestep (Wh)
η_E	The average quantum efficiency of the PV material
$\in$	wavelength dependant emissivity
H_{air}	Convective heat transfer coefficient of air ($W/(m^2K)$)
$I_{B.B.}$	Function that defines the ideal blackbody radiation spectrum ($W/(m^2\ \mu m)$)
I_{Solar}	Function that defines the global AM1.5 solar irradiance spectrum ($W/(m^2\ \mu m)$)
i	TEC operating current (A)
J_o	A coefficient that scales the magnitude of the solar irradiation throughout the day
K	Thermal conductance (W/K)
k	Thermal conductivity (W/(mK))
L	The precipitable water length in humid air (cm)
λ	Wavelength (μm)
n	An index variable for denoting the current timestep
p_{PV}	PV panel output power (W/m^2)
p_{TEC}	TEC power consumption (W/m^2)
ϕ	The power-temperature loss coefficient (/°C)
Q_{Load}	The instantaneous cooling load of the building room (W)
Q_P	The magnitude of heat radiated by a typical human body (W)
Q_{Wall}	Heat loss through the building walls (W)q_H - Heat flux at the TEC hot side (W/m^2)
q_L	Heat flux at the TEC cold side (W/m^2)
q_a	Convective heat flux on the PV panel's top surface (W/m^2)
q_b	Convective heat flux on the PV panel's bottom surface (W/m^2)
$q_{C(TEC)}$	TEC cooling flux (W/m^2)
$q_{C(RSC)}$	RSC cooling flux (W/m^2)
$q_{C(T)}$	Total cooling flux by the PV-RSC-TEC system (W/m^2)
q_r	Radiative heat flux into the outer space (W/m^2)
q_s	Solar irradiation flux that is absorbed (W/m^2)
σ	Electrical Conductivity (S/m)
T_{room}	Enclosed building space temperature (°C)
T_{amb}	Ambient temperature (°C)
T_{PV}	PV panel temperature (°C)
T_{sky}	Sky temperature (°C)
T_{dew}	Dew-point temperature (°C)
t	Time (s)
V_{room}	The volume of the building space (m^3)
z	The thickness of the building wall (m)

Constants

$c = 2.998 \times 10^8$ m/s Speed of light
$h = 6.626 \times 10^{-34}$ Js Planck's Constant
$k = 1.38 \times 10^{-23}$ J/K Boltzmann's constant

Subscripts and Superscripts

A	atmosphere
cell	Refers to properties related to the PV materials

work [12], which obtained heating COPs ranging within 3.27–3.45. Nevertheless, despite having a high performance, the PV-VCC system has a high system complexity because of the VCC's structure and the power electronics equipment needed to convert the PV's DC output into the AC input of the VCC.

Recognizing that reliability and structural simplicity are important factors, the thermoelectric cooler (TEC) has also been studied (i.e., PV-TEC system) [13] because it is fully solid-state and does not require toxic fluids. In particular, Daghigh and Khaledian [14] showed that a PV-TEC system could achieve a cooling COP of 1 and a stagnation cooling temperature of down to −3 °C. Moreover, Irshad et al. [15,16] constructed a building that combined the PV wall and the thermoelectric air duct system (the latter being based on their previous works [17,18]). By additionally including an air gap to remove the PV waste heat, this implementation lowered the room temperature to 6.8 °C below the outside ambient air. Unfortunately, as the TEC has a low COP, the PV-TEC system is currently a less preferable option than the PV-VCC system.

Besides, the PV-HP system's energy performance is also limited by the PV panel's electrical efficiency, which can be around 20% for cost-effective materials [19,20]. Thus, this technology has difficulty in achieving the performance needed for widespread commercial use. Alternatively, the cold outer space environment is another suitable heat sink for cooling, a concept utilized by radiative sky coolers (RSC). Radiative cooling works because room temperature (≈25 °C) blackbody radiation has a large spectral peak in the mid-infrared waveband (within 8–13 μm) range, and the same waveband is where the Earth's atmosphere has a high transmission and low absorption [21]. RSCs optimize this cooling effect by maximizing the emissivity within the mid-infrared waveband while minimizing it in other spectrums. However, despite being known to humanity for many centuries [22], its cooling density is extremely low (e.g. 100 W/m^2 [23]), which is very low over other cooling technologies even under the best possible working conditions (i.e. Low RH, clear night sky, temperature difference under 5 °C, etc.). Furthermore, conventional RSCs also cannot work during the daytime because of solar absorption; Although recent research has shown that daytime RSC is possible by maximizing the surface reflectance about the solar spectrum via specialized materials and structures (e.g., dual-layer structure RSC [24], the multi-layered titanium oxide [25], and the asymmetric electromagnetic transmission window (AEMT) method [26]), these materials are typically rare or difficult to manufacture. Hence, RSC is currently an uneconomical standalone technology and it is instead mostly used to supplement another cooling system. For example,

Muselli [27] and Zhang et al. [28] both demonstrated that the RSC can be integrated with the common air conditioner (usually the vapor compression cycle) and reduce the latter's energy consumption by up to 26–49%. Nevertheless, as this practice requires significant modifications and higher system complexity, its economic feasibility is still a significant concern.

Recently, the concept of integrating the RSC function during the nighttime and power generation by the photovoltaic (PV) effect during the daytime has gained much recent attention by numerous researchers, such as Zhao et al [21]. Notably, as discussed by Zhao et al. [29], the RSC function is a common cooling method for PV cells because conventional PV cells naturally already have this ability. This concept is verified by Riverola et al. [30] who showed that the atmospheric window emissivity of the common crystalline silicon solar cell is over 0.8. Therefore, the focus should be to optimize the RSC ability rather than to propose it. However, if the PV panel is required to produce power, then it cannot reasonably achieve daytime cooling because, unlike the daytime RSC, it cannot allocate reflection to the solar spectrum band (0.2–1.1 μm). According to the review report by Sato & Yamada [31], even when the radiative emissivity in the infrared band is perfectly 1, the RSC method could only achieve a further $1^{\circ}C$ temperature reduction to the PV panel during daytime operation. This is a major technological issue because cooling energy is generally at higher demands during the daytime than at nighttime. To tackle this major drawback, Zhao et al. [32] proposed a new strategy in which the PV panels are located at the building's sunny side, and RSC modules are located at the shady side; Hence, a combined electricity and cooling production system is formed. However, in comparison to a standalone PV system, this system required large amounts of floor space and high economic costs. Hence, it is more practical to redirect some of the PV-RSC output power into a heat pump technology to produce the daytime cooling energy. Furthermore, besides maximizing the cooling capacity of the cooling devices, minimizing the cooling loads of the building space by improving the building's insulation properties is another very common research direction [33,34]. The design process for the building's space cooling system should not only involve optimizing the cooling device, but it should also compare the output cooling performance to the building's cooling loads to properly couple these two parts together.

To overcome the low energy performance of the PV-TEC system, this paper proposes to integrate the PV panel's RSC ability into this system, thus forming a complete PV-RSC-TEC system. During the daytime, the PV-TEC component works as usual to produce cooling energy, but during the nighttime, the PV-RSC panel produces cooling power via the RSC effect. Hence, the RSC effect not only increases the overall cooling density under the same PV-TEC system size but also improves the temporal match between cooling supply and demand by enabling the TEC to allocate more cooling energy into the daytime period. To optimize the system, first, a realistic analytical spectral model that involves the emissivity spectrum of crystalline solar cells and Planck's law is developed to calculate the radiative flux of the RSC component, which is then coupled to the TEC model to evaluate the total cooling power of the PV-RSC-TEC system. Then, to achieve a good temporal match for cooling, two modes of how the PV power is supplied to the TEC is studied; The first is the TEC operates continuously at the time-averaged PV output power to provide cooling throughout the entire day (using a battery as a buffer), and the second is to directly feed the PV output power to the TEC during the daytime. To prove the feasibility of these modes of operation, a simplified cooling load model for an occupied building is developed, which is compared to the PV-RSC-TEC system's cooling capacity to evaluate the required PV surface area. This study is conducted by a time-dependent analysis using weather data for 7 typical days in Hefei, China.

2. System modelling

2.1. Overall structure

Fig. 1 shows the schematic and energy flow relationships of the proposed PV-RSC-TEC system, where (a) shows the case for daytime operation and (b) shows the case for nighttime operation. The PV-RSC panel is treated to be a regular flat PV panel where a transparent film covers the PV cells to form an air gap and minimize convective heat transfer (which still exists) with the ambient environment (q_a). Meanwhile, an airflow channel is placed directly below the PV-RSC panel, and the origin and destination of the flowing air are different between the daytime and nighttime. During the daytime, solar power (q_s) is incident to the PV-RSC panel to produce electricity (p_{pv}) and a large amount of waste heat, implying the PV-RSC panel cannot provide cooling energy. Thus, in this instance, air from the ambient environment is allowed to circulate along the airflow channel to maximize the ability to dissipate the waste heat into the ambient air. In contrast, during the nighttime, thermal radiation (q_r) becomes the relatively dominant energy flow, so a part of the produced cooling energy (q_b) can now be collected by circulating airflow. During this instance, the battery becomes the sole energy source for the TEC operation.

The combination of 1st law thermodynamics and the spectrum characteristics of the crystalline solar cell has been used to calculate the cooling energy, both in terms of the TEC via the produced electricity and the RSC. According to the principle of energy conservation, the following energy flow relationship on the PV-RSC panel is obtained for the daytime and nighttime cases:

$$\begin{array}{ll} q_s = q_r + q_a + q_b + p_{PV} & \textbf{Daytime} \\ q_{C(RSC)} = q_r + q_a & \textbf{Nighttime} \end{array} \quad (1)$$

Due to the different thermodynamic conditions, the PV panel temperature (T_{PV}) should be treated differently between the daytime and nighttime scenarios. During the daytime, T_{PV} should be calculated based on the daytime expression of Eqs. (1) whereas during the nighttime, it is assumed that T_{PV} equals T_{room}. From the above formulations, the cooling energy available to the building room space may be calculated as follows:

$$q_{C(T)}(t) = \begin{cases} q_{C(TEC)}(t) & \textbf{Daytime} \\ q_{C(TEC)}(t) + q_{C(RSC)}(t) & \textbf{Nighttime} \end{cases} \quad (2)$$

noting that t is time (s), which implies the cooling loads can vary with time depending on the ambient conditions and the selected TEC mode of operation. The following assumptions are made about the model analysis:

1. In practice, the waste heat at the TEC hot side should be dissipated into the ambient air. Thus, convective heat transfer theoretically exists here, and the TEC hot side surface temperature T_H will be at a higher value than T_{amb}. To simplify the calculation process, it will be assumed that sufficient convective cooling is provided to enable T_H to be 8 °C above T_{amb} [35].
2. Heat losses through the air gaps and physical connection points of the building walls are neglected.
3. The heat losses through the battery and the electrical wire resistances are assumed to be negligible.
4. Power losses through the involved power converters are small.
5. When the system switches from daytime to nighttime operation, the effect of any residual heat in the air duct below the PV-RSC panel is ignored.

2.2. Modes of operation

In this paper, two different modes of operation for the PV-RSC-TEC system will be studied, each of which handles the temporal

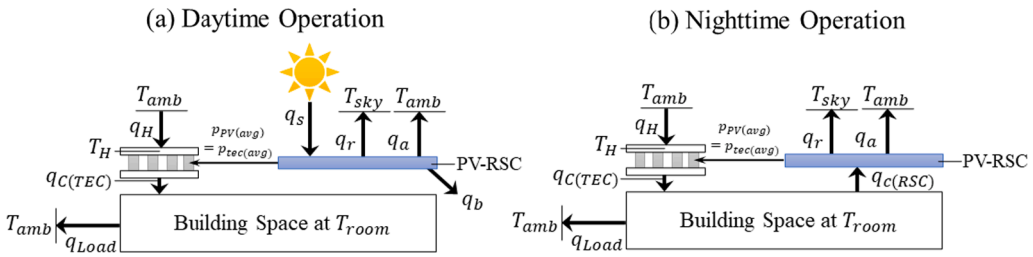

Fig. 1. Overall structure of the PV-RSC-TEC hybrid cooling system that illustrates the heat flow relationships.

distribution of the cooling demand and supply differently. These two modes have been graphically illustrated in Fig. 2, and their detailed description is provided in the smaller subsections.

For both modes of operation, the required PV surface area is determined by comparing the cooling demand and supply at each instantaneous moment:

$$A_{req}(t) = \frac{Q_{Load}(t)}{q_{C(T)}(t)} \tag{3}$$

where $Q_{Load}(t)$ is the instantaneous cooling load of the building room, whose formulation is provided in Section 2.7; $q_{C(T)}$ is the instantaneous total supply of cooling energy as presented in Eqs. (2). Then, the largest $A_{req}(t)$ value (i.e. $\max(A_{req}(t))$) should ideally be chosen to satisfy all the entire day's range of cooling loads.

2.2.1. Include electric battery

In the first mode, a battery is used to buffer the incoming solar energy into an all-day time-averaged constant for the TEC. In this case, p_{TEC} is evaluated as follows:

$$p_{TEC}(\textbf{Mode}1) = \frac{\int_0^{t_{total}} p_{PV}(t)dt}{t_{total}} \tag{4}$$

where t_{total} denotes 24 h. This mode shall namely be the continuous TEC mode.

To estimate the battery size needed to support the continuous TEC mode, first the amount of stored energy e_{bat} is initiated to zero at the beginning of the time simulation. Then, the change of e_{bat} after a certain time-step (n, the time step size is selected as 1 h) with $p_{pv}(t)$ and $p_{TEC}(t)$ is calculated as follows:

$$e_{Bat}(n+1) = e_{Bat}(n) + \left(p_{pv}(t) - p_{TEC}(t)\right)\Delta t \tag{5}$$

From this, the required battery size is defined as the difference between the maximum and minimum magnitudes of this stored energy within the studied timeframe:

$$E_{Bat} = \max(e_{Bat}) - \min(e_{Bat}) \tag{6}$$

2.2.2. d-TEC:n-RSC

In the second mode, the PV output power is directly given to the TEC to support the daytime cooling demand, so $p_{TEC}(\text{Mode2})(t) = p_{PV}(t)$. During the nighttime, the cooling demand is solely supplied by the RSC only. This mode would not require a battery so it may be more economical than the first mode. This mode shall namely be the "d-TEC:n-RSC" mode. After computing p_{TEC}, the TEC cooling power $q_{C(TEC)}$ can be calculated accordingly.

Optionally, a thermal storage device can be used to support the "d-TEC:n-RSC" mode by allowing a better temporal match of the cooling load versus supply throughout the day. This special situation can reduce the PV area requirement because, unlike Eqs. (3), the area requirement can now be based on the daily average cooling demand and supply instead, as calculated below:

$$A_{req(T.S.)} = \frac{\int_0^{24hr} Q_{Load}(t)dt}{\int_0^{24hr} q_{C(T)}(t)dt} \tag{7}$$

Then, the corresponding thermal storage device size can be calculated using a similar methodology as that shown in Eqs. (5) and (6) except that the $Q_{Load}(t)$ and should be applied in the formula, as shown below:

$$e_T(n+1) = e_T(n) + \left(A_{req(T.S.)}q_{C(T)}(t) - Q_{Load}(t)\right)\Delta t \tag{8}$$

$$E_T = \max(e_T) - \min(e_T) \tag{9}$$

2.2.3. Analysis method

After selecting the mode of operation, the following design methodology is used to calculate the maximum available cooling power and the required PV area ($A_{(req)}$) by the proposed system:

1. Consider a certain commercial PV panel and TEC module. Calculate the instantaneous $p_{PV}(t)$ throughout the time of day, and hence calculated $p_{TEC}(t)$ depending on the operational mode choice.
2. Use the TEC model to calculate the corresponding TEC cooling power ($q_{C(TEC)}(t)$).

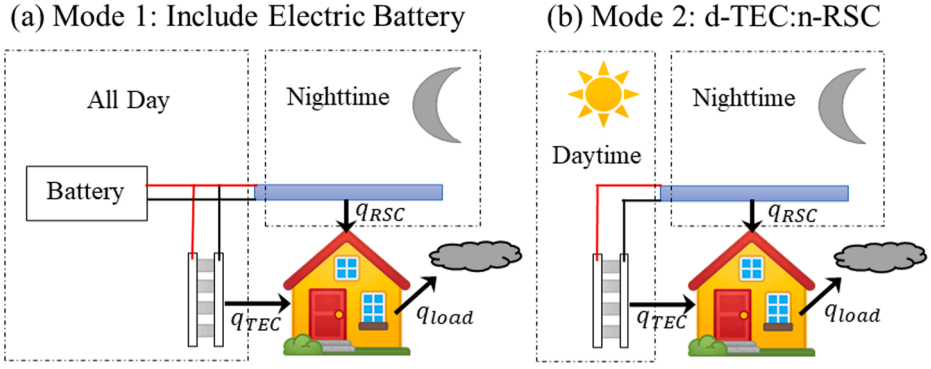

Fig. 2. The two different modes of operations that will be studied in this paper.

3. Calculate the yieldable RSC cooling power ($q_{C(RSC)}(t)$) by using the spectrum analysis model.
4. Calculate the total cooling power $q_{C(T)}$ as the sum of the RSC and TEC cooling power.
5. Based on Eq. (3), calculate $A_{PV(req)}$ given a value of k_{wall} and z.

After the cooling powers are known, the equivalent solar to cooling energy COP can be calculated as follows:

$$\boldsymbol{COP_{Eq}} = \frac{\int \boldsymbol{q_c dt}}{\int \boldsymbol{q_s dt}} \tag{10}$$

where the integration should cover the entire day and the term q_c can be substituted to be any cooling variable, such as $q_{C(TEC)}$ for cooling by TEC only or $q_{C(T)}$ for total cooling power. The individual simulation models needed to carry out the above methodology are described in the following subsections.

2.3. Spectral analysis

In Eqs. (1), q_S is the absorbed incident solar power, which is defined as follows:

$$\boldsymbol{q_S} = \boldsymbol{J}_0(\boldsymbol{t}) \int_0^\infty \in_{\boldsymbol{Cell}}(\boldsymbol{\lambda}) \boldsymbol{I_{Solar}}(\boldsymbol{\lambda}) \boldsymbol{d\lambda} \tag{11}$$

where $J_0(t)$ is a coefficient that scales the magnitude of the solar irradiation throughout the day, $\in_{Cell}(\lambda)$ is the emissivity spectrum of the PV material, and $I_{Solar}(\lambda)$ is the global AM1.5 solar irradiance spectrum. The wavelength dependant curves $\in_{Cell}(\lambda)$ and $I_{Solar}(\lambda)$ have been graphically illustrated in Fig. 3, where $\in_{Cell}(\lambda)$ was taken from the experimental study by Riverola et al. [30] for crystalline silicon (c-Si). Meanwhile, the solar panel emits radiative thermal power into outer space by the following equation:

$$\boldsymbol{q_r} = \int_0^\infty \in_{\boldsymbol{Cell}}(\boldsymbol{\lambda}) \boldsymbol{I_{B.B.}}(\boldsymbol{\lambda}, \boldsymbol{T_{PV}}) \boldsymbol{d\lambda} - \int_0^\infty \in_{\boldsymbol{A}}(\boldsymbol{\lambda}) \boldsymbol{I_{B.B.}}(\boldsymbol{\lambda}, \boldsymbol{T_{amb}}) \boldsymbol{d\lambda} \tag{12}$$

where T_{PV} is the PV panel's temperature, and T_{amb} is the ambient air temperature. In this equation, the left term denotes the radiative flux from the PV material whereas the right term denotes the received thermal radiation from the atmosphere. Here, $I_{B.B.}(\lambda, T)$ is the spectral-dependant energy distribution of the blackbody as depicted by Planck's law:

$$\boldsymbol{I_{B.B.}}(\boldsymbol{\lambda}, \boldsymbol{T}) = \frac{2\boldsymbol{\pi hc}^2}{\boldsymbol{\lambda}^5 (\boldsymbol{e}^{\frac{\boldsymbol{hc}}{\boldsymbol{\lambda kT}}} - 1)} \tag{13}$$

Also, $\in_A(\lambda)$ is the radiative emissivity of the atmosphere, which is practically a complex curve that depends on the specific constituents of the air. Based on Zhao et al. [30], the atmospheric emissivity, while having many uncertain variations, is generally at or close to 1 in the ranges $4\ \mu m \le \lambda < 8\ \mu m$ and $\lambda > 13\ \mu m$. For the wavelengths within the solar spectrum, it can be roughly estimated by using the ratio difference in the spectral irradiance between AM0 and AM1.5 Global irradiation (raw data can be found in [36]). Meanwhile, the atmospheric emissivity within the atmospheric window ($8\ \mu m \le \lambda < 13\ \mu m$) is highly dependent on the water content in the air (i.e., RH). Thus, in this paper, the atmospheric emissivity is approximated as follows:

$$\in_A(\lambda) = \begin{cases} 1 - \frac{I_{Solar(AM1.5)}}{I_{Solar(AM0)}} & \lambda < 4\ \mu m \\ 1 & \lambda < 8\ \mu m, \lambda > 13\ \mu m, \\ \in_{A(0)} & 8\ \mu m \le \lambda \le 13\ \mu m \end{cases} \tag{14}$$

where according to Zhao et al. [30], $\in_{A(0)}$ is another complex curve, but an overall average in terms of RH can be estimated. To simplify the calculation process, this paper will assume that $\in_{A(0)}$ is constant in terms of λ, and its value will vary with RH and will as closely mimic the curves shown by Zhao et al. [30] as possible. Specifically, the following empirical expression is used to estimate $\in_{A(0)}$:

$$\in_{\boldsymbol{A(0)}} = 0.0007\boldsymbol{L}^3 - 0.0144\boldsymbol{L}^2 + 0.1457\boldsymbol{L} + 0.0853 \tag{15}$$

where L is the precipitable water length (cm), which can be found by the following empirical formula:

$$\boldsymbol{L} = \frac{1}{10}\left(0.06\boldsymbol{T}_{\boldsymbol{amb}}^2 - 0.05\boldsymbol{T}_{\boldsymbol{amb}} + 11\right)\mathbf{RH} \tag{16}$$

where the T_{amb} is valid in the range of ($0^\circ C \leqslant T_{amb} \leqslant 40^\circ C$), noting that in this formula, the units shall be °C. Also, the RH units shall be the absolute value (i.e. 0–1).

2.4. Convective heat transfer

The convective heat transfer expressions q_a and q_b may be calculated as follows:

$$\boldsymbol{q_a} = \boldsymbol{H_{air(1)}}(\boldsymbol{T_{PV}} - \boldsymbol{T_{amb}}) \tag{17}$$

$$\boldsymbol{q_b} = \begin{cases} \boldsymbol{H_{air(2)}}(\boldsymbol{T_{PV}} - \boldsymbol{T_{amb}}, & \textbf{Daytime} \\ \boldsymbol{q_{C(RSC)}}, & \textbf{Nighttime} \end{cases} \tag{18}$$

where $H_{air(1)}$ and $H_{air(2)}$ are the convective heat transfer coefficients on the top and bottom surfaces of the PV-RSC panel, respectively. For $H_{air(1)}$ which exists all day and night, efforts to suppress its influence is possible

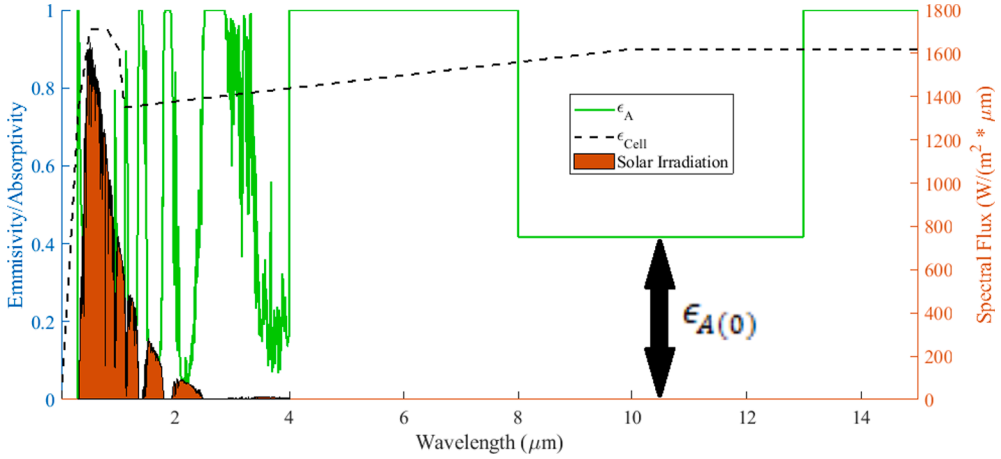

Fig. 3. The emissivity spectrum of the atmospheric air ($\in_A$), the solar cell ($\in_{Cell}$), and the radiation spectrum of AM1.5 solar power.

by covering the PV surface with a transparent film [37], so a relatively small equivalent value of $1W/(m^2K)$ is chosen. Notably, q_a will exist throughout the entire day since the PV panel is always facing the sky. For $H_{air(2)}$, a value of $10W/(m^2K)$, which is typical of natural convective cooling [38], is set during the daytime for the PV panel's bottom surface. However, during the nighttime, the PV panel's bottom surface directly interfaces with the building room by natural circulating air. Hence, q_b is calculated by thermodynamic balance to be equal to $q_{C(RSC)}$.

2.5. PV panel efficiency

Theoretically, the PV-RSC panel can only convert a certain portion of the adsorbed energy q_s into electricity, which depends on the bandgap selectivity of the PV material. In this paper, the average quantum efficiency of the solar cell η_E will be used to obtain p_{PV} as shown below:

$$p_{PV} = \eta_E q_S \tag{19}$$

where η_E is estimated by using the electrical efficiencies reported by commercial PV panel datasheets. Furthermore, η_E is also known to drop with increasing PV temperature, a factor that is taken into account below:

$$\eta_E = \eta_{E(0)}[1 + \phi(T_{PV} - T_0)] \tag{20}$$

Here, ϕ is the power-temperature loss coefficient (ratio/ °C), and the terms subscripted with 0 denote the manufacturer specified values of the PV material.

2.6. TEC model

The widely known energy equilibrium TEC model described in [5,39] is adopted here, and the model equations are shown below:

$$q_H = n[\alpha i T_H + \frac{\lambda A_{tc}}{l_{tc}}(T_H - T_1) - \frac{1}{2}i^2\frac{l_{tc}}{\sigma A_{tc}}] \tag{21}$$

$$q_{C(TEC)} = n[\alpha i T + \frac{\lambda A_{tc}}{l_{tc}}(T_H - T_1) + \frac{1}{2}i^2\frac{l_{tc}}{\sigma A_{tc}}] \tag{22}$$

where $q_{C(TEC)}$ is the contribution of cooling energy by the TEC; q_H is the heat that is dissipated into the ambient environment; A_{tc} is the combined surface area of a single thermocouple pair; l_{tc} is the length of the thermocouples in the heat flow direction; T_H is the TEC hot side temperature. The TEC power consumption is evaluated as follows:

$$p_{TEC} = q_H - q_L \tag{23}$$

In these equations, the Seebeck coefficient α, electrical conductivity σ, and thermal conductivity λ parameters will vary with the thermocouple's operating temperature [5]. However, because this paper studies the TEC when it operates in a relatively small temperature range about the natural ambient condition, constant values have been assumed. The values used in our previous publication [39] have been directly reused here, which are: $\alpha = 4.5313 \times 10^{-4}$ V/K, $\sigma = 1.7150 \times 10^5$ S/m and $\lambda = 3.162$ W/(mK).

2.7. Cooling load model

To evaluate the feasibility of the PV-RSC-TEC system, a simplified model is used to estimate the cooling loads of an occupied building and subsequently the PV area required to satisfy this. Minimizing the building's cooling loads (often known as energy-efficient buildings design) is another popular research trend for minimizing the size requirement of the applied cooling system [40]. However, the building's cooling load involves numerous factors such as the building's structural design, the number of occupants, and the operations conducted inside the building, etc., so it is very complex and uncertain. To minimize the model complexity, this paper considers heat radiated by the human body (Q_P) and heat loss through the building walls (Q_{wall}) as the primary cooling loads, which are defined as follows:

$$Q_{Load} = Q_P + Q_{wall} \tag{24}$$

where Q_{wall} can be defined as:

$$Q_{wall} = \frac{kA_{wall}}{z}(T_{amb} - T_{room}) \tag{25}$$

where k_{wall} is the thermal conductivity of the wall (W/(m °C)); z is the thickness of the wall (m), and A_{wall} is the surface area of the walls (m^2). In this paper, the room is set to be a rectangular prism so the A_{wall} value includes the 4 walls and the ceiling whereas the ground is excluded. Notably, by setting the outside wall temperature as T_{amb}, this implies that the outside wall's convective heat transfer ability is perfect. Although this may not be true in reality, this assumption will maximize the size of the cooling load Q_{wall}, which is suitable for achieving a conservative analysis of the cooling system. The building's summary specifications have been listed in Table 1 and have been described in detail under Section 4.

2.8. Time-dependent analysis

This paper aims to analyze how the PV-RSC-TEC hybrid system performs in a real-time environment with varying conditions. The time-varying data shown in Fig. 4 for Hefei city, China, has been chosen for the analysis.

The average cooling power throughout the daytime and nighttime periods are useful parameters for assessing the average performance of the PV-TEC-RSC system, which are calculated as follows:

$$q_{C(day)} = \frac{\int^{t_{day}} q_{C(T)} dt}{t_{day}} \tag{26}$$

$$q_{C(night)} = \frac{\int^{t_{night}} q_{C(T)} dt}{t_{night}} \tag{27}$$

3. Model validation

To show that the presented models are accurate, the TEC and RSC models are first validated through comparisons with experimental data from previous publications. Notably, the TEC model has already been validated in our previous publication [39], and we have directly reused that TEC model in this paper. The RSC model is then validated in the following content through a comparison with the results obtained by Zhao et al. [22]. In Zhao et al.'s study, the cooling power versus temperature curve was reported for a high-performance polyvinylidene fluoride-based RSC panel under a variety of h_{air} values. Here, we specifically took $h_{air} = 8\ W/(m^2\ K)$ as the sample value because its order of magnitude is the same as those in the main analyzes of this paper. Furthermore, the PVDF's emissivity spectrum was reported there and is reapplied to the present model to validate it. Fig. 5 shows the comparison of the radiative cooling power results obtained between the two models, which shows a good agreement at lower temperature

Table 1
The building space specifications.

Parameter	Value
Number of Occupants	4
Room dimensions	2.5 m (height) × 4 m (length) × 6 m (width)
Corresponding wall area (A_{wall}), floor area (A_{floor}) and volume of the room (V_{room})	74 m^2, 24 m^2, and 60 m^3, respectively
The thickness of the room's walls (l)	0.1 m
The thermal conductivity of the room's walls (k_{wall})	0.1 W/(m °C)

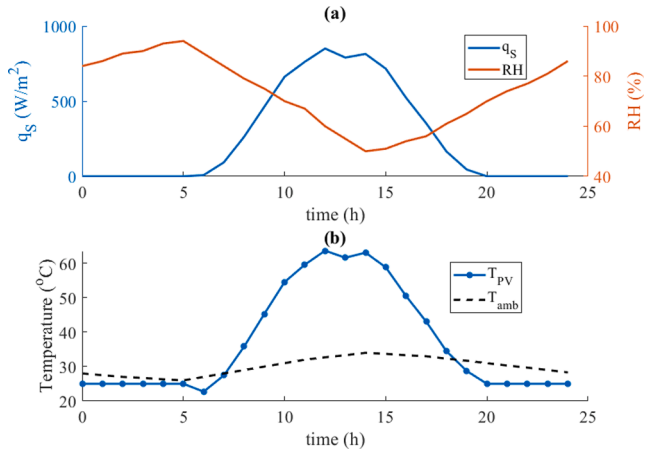

Fig. 4. Time-dependent environmental characteristics of Hefei on day 29,800 (a) Global direct solar irradiance (q_S) and the ambient RH (b) Ambient temperature and corresponding PV panel temperature.

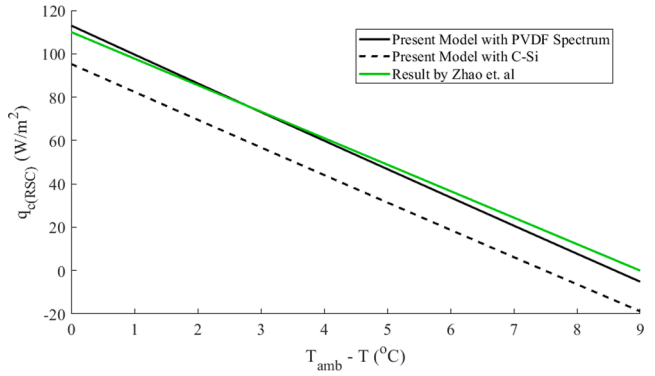

Fig. 5. Comparison of the retrievable cooling power result between the present model and that from Zhao et al. [22] when a PVDF panel is used and $\mathbf{h_{air}} = 8\ \mathbf{W/(m^2K)}$.

differences ($< 7.5^{\circ}C$). A slight deviation is observed at the higher values, which is most likely because of the discrepancy in calculating the atmospheric radiative power between the two models. Nevertheless, this deviation is not large. Furthermore, Fig. 5 also shows the net radiative power result by the present model when the c-Si's emissivity spectrum is used instead, which are clearly shown to be lower than the PVDF panel. This is expected because, as shown in Fig. 3, c-Si's emissivity spectrum involves values that typically range between 0.7 and 0.9, which are less ideal than the PVDF panel. Hence, it is verified that the present RSC model is reasonably accurate.

4. Simulation parameters

Space cooling of a small building room during the summer has been chosen as the target objective of this paper, where the temperature difference ($T_{amb} - T_1$) could range between 3 °C and 10 °C. Specifically, the room has 4 occupants, and it is assumed each occupant radiates 100 W of body heat [41] (i.e. $Q_P = 400$ W). The key specifications of the studied building space have been summarized in Table 1, and the cooling load profile for the studied room is depicted in Fig. 6. Indeed, a larger building wall area and the increasing number of occupants would increase the cooling demand size. Notably, according to Fig. 6, together with the building wall surface area, the $T_{amb} - T_1$ difference impacts the cooling demand much more than the number of occupants. Hence, the PV-TEC-RSC system size is likely higher for a more spacious building.

Table 2 lists the other working conditions that have been imposed in this paper. The commercially available crystalline silicon (c-Si) solar cells are chosen as the PV material because it has both a reasonably high emissivity within the atmospheric window and can also yield a reasonable enough power efficiency for the TEC [42]. Natural convective cooling has been assumed in the paper, hence resulting in the choices shown in Table 2.

Meanwhile, a commercial TEC module is applied in this paper whose specifications have been summarized in Table 3. Given that the geometrical parameters are fixed, there exists a maximum COP with respect to the input TEC power because of the balance between the increase of the Peltier effect and increasing resistive losses. A brief inspection reveals that 4 TECs per m^2 of PV panel would yield the highest COP, so we utilize this rate (all serially connected) in all of the analyzes. Notably, since the RSC cooling power is directly proportional to the PV panel size, this means that the cooling power ratio between the RSC and the TEC will be relatively constant regardless of the overall PV-RSC-TEC system size.

Table 2
List of the working conditions that are imposed in this paper's study.

Parameter	Value
Solar Panel Nominal Efficiency (η_E) and Output Power Density (p_{pv}) [42]	20% & 120 W/m^2
Convective heat transfer coefficient at the PV-RSC panel's top surface	$H_{air(1)} = 1$ W/(mK)
Convective heat transfer coefficient at the PV-RSC panel's bottom surface	$H_{air(2)}$ { 10 $W/(mK)$, *Daytime*; 0 $W/(mK)$, *Nighttime*

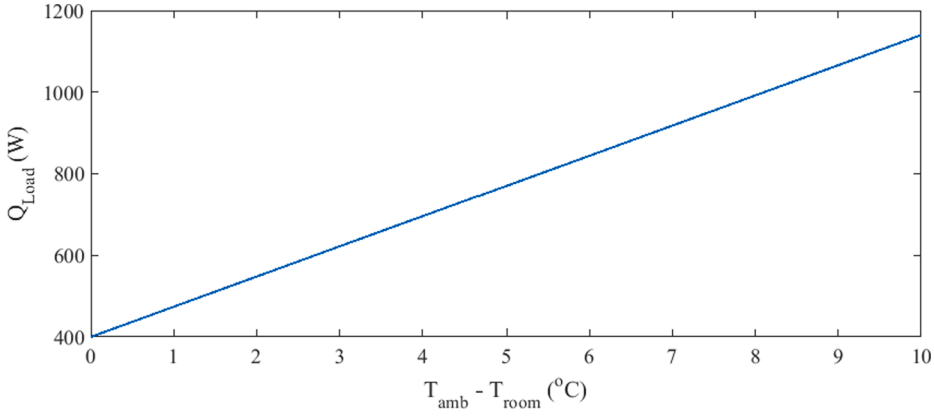

Fig. 6. Adopted profile of Q_{Load}, which is based on involving 4 people in the room while $z = 0.1$ m and $k_{wall} = 0.1$ W/(m K).

Table 3
List of the TEC specifications as used in this paper.

Parameter	Value
Commercial TEC Product [43]	TEC1-12715 (4 cm by 4 cm module)
Mass of the TEC module	15 g
thermocouple length (l_{tc})	1 mm
Combined thermocouple pair cross-sectional surface area (A_{tc})	2 × 1.2 mm by 1.2 mm
The number of TEC modules per unit area of PV surface.	4 modules/m^2

5. Results

In the following analysis, the building's room temperature (T_{room}) is first fixed at the target of 25 °C, which can be regarded as the maximum acceptable room temperature for summer [44]. Then, the ambient temperature, ambient RH, and magnitude of solar irradiance are all varied according to Hefei on Day 29,800 (Fig. 4). By using these as inputs, the available cooling powers by the TEC and RSC as well as the building's cooling load can be calculated at each hour of the day. Based on these results, the theoretical PV area requirement (A_{req}) to meet the cooling load at each instance of time can be estimated, which indirectly implies the economic feasibility of the PV-RSC-TEC system. After this, the PV-RSC-TEC system's cooling power performance is then analyzed over 1 week in Hefei (days 29,800–29,806) to prove its stability under different weather conditions. Based on these results, a reasonable A_{PV} value is selected and T_{room} becomes a time varying value and is monitored to verify the system's cooling ability.

5.1. Time-dependent characteristics

Fig. 7 shows how the TEC, RSC, and total cooling powers vary with time for the two modes of operations in each respective subplot. Based on Fig. 7 (a), clearly, $Q_{C(TEC)}$ is relatively stable at around 50 W/m^2, which is normal because the P_{TEC} is fixed in this instance. Here, the slight variations are because of the varying T_{amb} throughout the day. During the nighttime, cooling by the RSC ($Q_{C(RSC)}$) was only around 60 W/m^2, and the TEC enhanced the total nighttime cooling power to around 120–130 W/m^2. As a result, in the continuous TEC mode, the PV-RSC-TEC system will yield a relatively constant $Q_{C(T)}$ that exhibits an almost "step" change between the daytime and nighttime periods. For the d-TEC:n-RSC mode, based on Fig. 7 (b), clearly the instantaneous $Q_{C(TEC)}$ is much higher than in the continuous TEC mode (up to 70–80 W/m^2), and this lasts for the duration between 9 am and 4 pm of the day. However, during the sunrise and sunset periods, $Q_{C(TEC)}$ will typically drop below 40 W/m^2 since the available P_{PV} is low at these times. Meanwhile, although $Q_{C(RSC)}$ is around 60 W/m^2 during the nighttime period, its value is also very weak during the sunrise and sunset periods because the solar irradiation is still present. As a result, the $Q_{C(T)}$ value during the sunrise and sunset periods is low, and this is a major disadvantage of using the d-TEC:n-RSC mode.

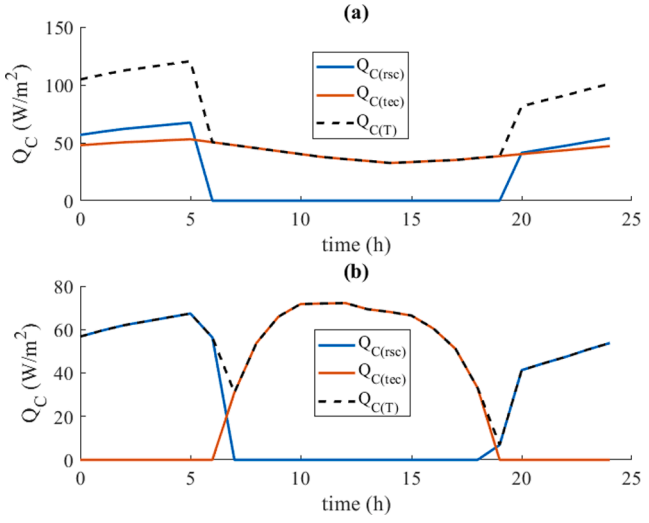

Fig. 7. The cooling power produced with the time on Hefei day 29,800 for (a) The continuous TEC mode (b) The d-TEC:n-RSC mode.

Based on the cooling power results of Fig. 7 and the cooling load model, the estimated minimum PV area (A_{req}) is calculated by using Eq. (3) and is reported in Fig. 8 for the two operational modes. Indeed, as the continuous TEC mode supplied a large magnitude of nighttime cooling power and that the nighttime cooling load is relatively low (due to a smaller $T_{amb} - T_{room}$ difference), its A_{req} is very low during the nighttime period. However, the A_{req} value during the mid-day has risen to up to 30 m^2, which indicates the available daytime cooling energy is not very well matched with the daytime cooling loads. Thus, the continuous TEC mode's nighttime cooling power is excessively high while the daytime cooling power is too low, which indicates a poor temporal match of the cooling energy.

For the d-TEC:n-RSC operational mode, its main advantage over the continuous TEC mode is the increased daytime cooling power that allowed for a much lower mid-day A_{req} requirement. However, due to the lack of available cooling power during the sunrise and sunset, the A_{req} during these times would spike to unrealistic values (e.g. 130 m^2 at 7 pm) which are indeed not realistic to cover economically. Thus, if the d-TEC:n-RSC operational mode is used, then the lack of available cooling power that arises during the sunrise and sunset periods is very likely needed to be tolerated by the end-user. Notably, such an issue can be resolved by including a thermal storage device to buffer the available cooling power and hence supplement the cooling demands at these sunrise and sunset periods. A brief inspection would reveal that adding thermal storage can lower the average A_{req} value down to 13.97 m^2. The corresponding required thermal storage size is about 961.32 Wh, which equates to roughly 18.21 kg of paraffin (the latent heat of fusion is 190 kJ/kg [45]). Thus, thermal storage inclusion is certainly a solution to solve the aforementioned lack of available cooling power problem during these two specific periods.

5.2. One week performance analysis

The previous section analyzed the PV-RSC-TEC hybrid system's performance based on a time profile of a single day. In this section, the analysis has been repeated to calculate the system's cooling performance under 7 consecutive days to prove that it can work under a wide range of different ambient conditions. Fig. 9 shows specifically the varying T_{amb} (in (a)), RH and q_s conditions for the selected 7 days.

Fig. 10 shows the average cooling powers over 7 consecutive days for

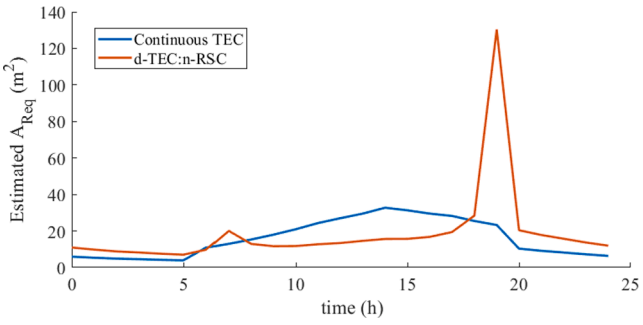

Fig. 8. The corresponding A_{req} of the PV panel to meet the cooling demands (a) Estimated value at each moment (b) The maximum A_{req} which will satisfy all the cooling needs.

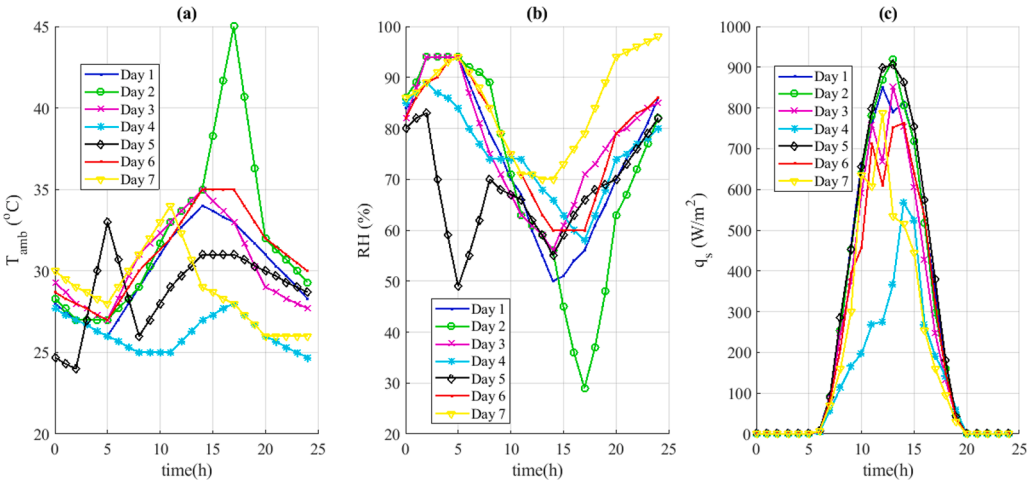

Fig. 9. The ambient conditions of the 7 consecutive days for the study.

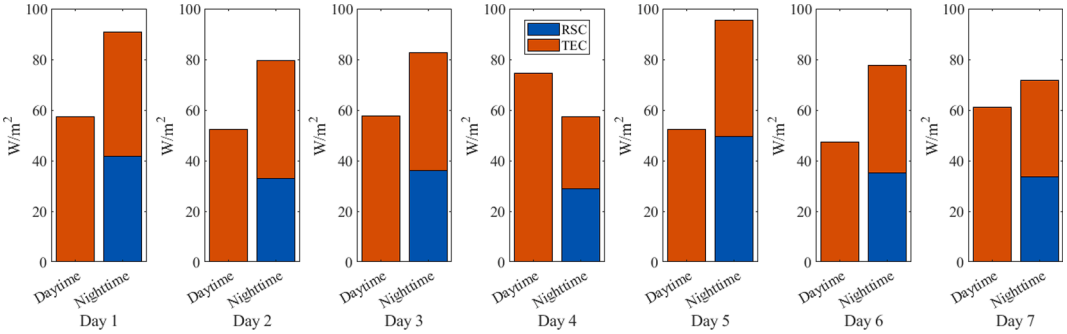

Fig. 10. The average daytime ($q_{C(day)}$) and nighttime ($q_{C(night)}$) average cooling powers obtained for each day of a full week using the continuous TEC mode.

the continuous TEC mode, which shows that the average daytime and nighttime cooling powers can vary considerably under different weather conditions. Here, it is shown that daytime cooling power will normally vary between 45 W/m^2 and 60 W/m^2, but an outlier on day 4 exists with a value reaching 74 W/m^2. This is interesting because, according to Fig. 9, the solar irradiance on day 4 is the lowest. The main reason for the increased available daytime cooling power is because, as seen in Fig. 9 (a), T_{amb} is very close and sometimes even lower than the setpoint T_{room} of 25 °C, so it is easy to produce large amounts of cooling energy. In contrast, despite having a higher irradiance, the daytime cooling power is much lower on days 2 and 6 where the daytime T_{amb} is mostly much higher than $T_{room} = 25^{\circ}C$, thus indicating that T_{amb} has a much stronger influence on the proposed system's cooling performance than the solar irradiance itself. Furthermore, because the primary reason for a higher T_{amb} is higher solar irradiance, this indirectly implies that a higher solar irradiance actually causes more stress on the proposed system's cooling requirement.

Meanwhile, the average nighttime cooling power also varies on different days, with values ranging between 60 W/m^2 and 95 W/m^2. In terms of the RSC, the primary contributing factor is the air RH; The RH was relatively low (with a lower peak of 50%) on day 5 to yield a higher $q_{C(RSC)}$ whereas on day 2, a consistent nighttime RH of 90% greatly lowered the $q_{C(RSC)}$ value. Meanwhile, a lower daytime irradiance naturally results in less $q_{C(TEC)}$ during the nighttime; For example, it was only about 30 W/m^2 on day 4 (with low average irradiance) while it was up to 45 W/m^2 on day 5. Overall, in the continuous TEC mode, the RSC and TEC performances for nighttime cooling are both highly affected by the ambient RH and solar irradiance conditions, respectively.

Fig. 11 shows the corresponding average daytime and nighttime cooling powers over the same 7 days but when the d-TEC:n-RSC mode is used instead. When compared to the results of Fig. 10, clearly the available nighttime cooling power is much lower since the d-TEC:n-RSC

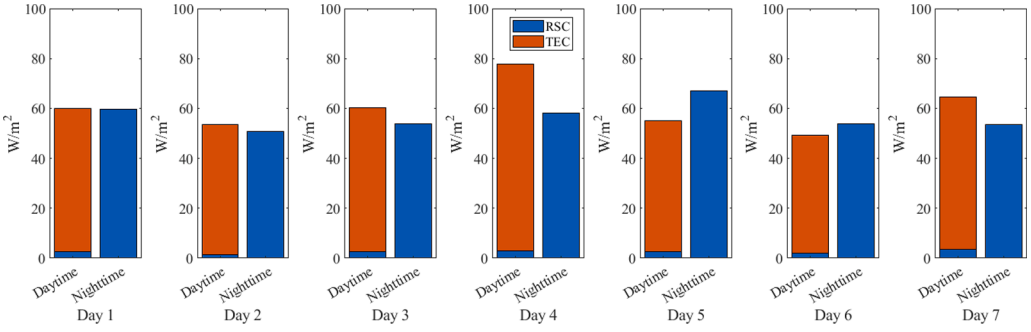

Fig. 11. The average daytime ($q_{C(day)}$) and nighttime ($q_{C(night)}$) average cooling powers obtained for each day of a full week using the d-TEC:n-RSC mode.

mode does not involve any TEC cooling power during this period. Meanwhile, the average daytime cooling power by the d-TEC:n-RSC mode is generally slightly higher than the continuous TEC mode although not by any significant margin. Other than this, except for day 4, the daytime cooling performance appears to be similar to the continuous TEC mode in which the daytime cooling performance mostly ranges between 50 W/m^2 − 65 W/m^2.

Fig. 12 shows the average A_{req} result for the two modes of operations, obtained by first using the time-averaged value ($\frac{\int^{t_{day}} A_{req}dt}{t_{day}}$ and ($\frac{\int^{t_{night}} A_{req}dt}{t_{night}}$) for each day, and then averaging again the obtained values from the 7 days of operation. Surprisingly, despite only having a very small increase in the average daytime cooling power, the average A_{req} for the d-TEC:n-RSC mode during the daytime is considerably lower than the continuous TEC mode (up to 1.6 times smaller). This demonstrates that, during this period, the d-TEC:n-RSC mode's instantaneous cooling power versus the cooling load profile ratio is much better matched than the continuous TEC mode.

During the nighttime, the continuous TEC mode has a very low average A_{req}, which indicates that this mode produces excessive nighttime cooling energy while not producing sufficient cooling energy during the daytime. Meanwhile, for the d-TEC:n-RSC mode, the average A_{req} between the daytime and nighttime is more closer together, indicating once again that the instantaneous cooling power production is better matched with the cooling load. Now recall from Table 1 that the studied room's floor space is 24 m^2. By comparing this value with those in Fig. 12, it seems only the d-TEC:n-RSC mode can meet the requirement that the PV panel area can be less than the room's floor space.

For the continuous TEC mode, the sizing requirement to meet most of the daytime cooling loads is a significant concern, which occurred because the distribution of cooling power between the daytime and nighttime is not well-matched with the cooling load. To resolve this problem, two possible strategies are suggested. The first is to introduce two-step values for the TEC's operating power, where the nighttime involves a lower value and the daytime has a higher value. Doing so can effectively "smooth out" the A_{req} curve in Fig. 8, which can lower the maximum peak during the mid-day and increase the economic feasibility of the PV-TEC-RSC hybrid system. The second strategy is to include a heat storage medium (e.g., phase change material) into the system to carry the nighttime cooling energy into the daytime. Nevertheless, this strategy is not recommended for the continuous TEC mode because it would further increase the economic cost on top of the already required battery.

5.3. Performance-based on a selected A_{PV}

In the previous analyzes, T_{room} was set to a constant value of 25 °C and the corresponding cooling load powers and required PV area (A_{req}) were calculated to meet this requirement. However, in reality, the PV area cannot be a "variable", and one has to set and implement a fixed PV area. Thus, this section performs a time-dependent analysis where the PV area is given and the parameter T_{room} can now vary with time. Based on the discussion relating to Fig. 12, the average A_{req} is in the same order of magnitude as the studied room's floor space. Thus, in this section, the PV area is set to be the same as the building's room floor space (i.e. 24 m^2) to represent a case that can be technically and economically implemented.

Fig. 13 shows the corresponding temperature results for the two modes of operation. Indeed, for the continuous TEC mode, during the nighttime, the temperature difference could be up to 10 °C which caused the room temperature to drop below 20 °C. This indicates that there is too much cooling energy being produced. In contrast, during the daytime, the temperature difference was only around 6.6 °C (e.g., at 2 pm, T_{room} was 27.44 °C while T_{amb} was 34 °C), so the cooling performance is somewhat lower. Overall, although the PV-RSC-TEC system can achieve the required cooling performance under this mode, the performance is certainly not optimal as there is too much cooling energy during the nighttime but not quite enough during the daytime. A thermal storage device may be required here to better balance this temporal mismatch problem.

For the d-TEC:n-RSC mode, during the nighttime, T_{room} would remain in the range of 20 °C to 22 °C, which indeed are more appropriate values in the building cooling application. These results suggest that the RSC is typically already enough for nighttime cooling, and adding the contribution by the TEC is not critically needed though still helpful on warmer days. Meanwhile, during the daytime, unlike the continuous TEC mode, T_{room} could remain in the 20 °C to 22 °C range, hence demonstrating that the d-TEC:n-RSC mode can achieve a better daytime cooling performance. Unfortunately, the d-TEC:n-RSC mode exhibits a spike in T_{room} at the sunrise and sunset moments, which is consistent with the observations found in Fig. 7 (b). Thus, installing the thermal storage device to buffer the supplied cooling power is recommended if these temperature peaks are not desired.

5.4. Discussion

Estimated the minimum theoretical battery size required to achieve the results in Fig. 12 (a) by the continuous TEC mode is 134.9 Wh/m^2 or 3.237 kWh for A_{PV} = 24 m2. These values are based on assuming that the battery is 100% efficient which indeed is not realistically possible.

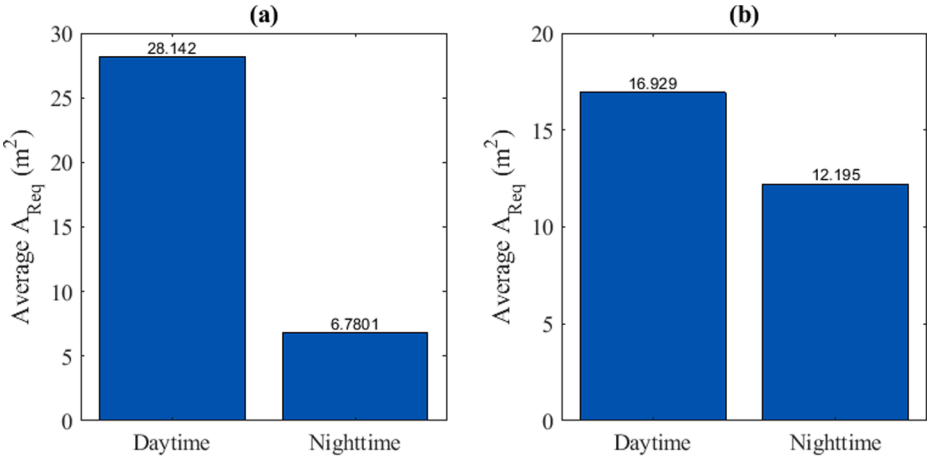

Fig. 12. The average A_{req} based on the 7 days of operation by (a) The continuous TEC mode (b) The d-TEC:n-RSC mode.

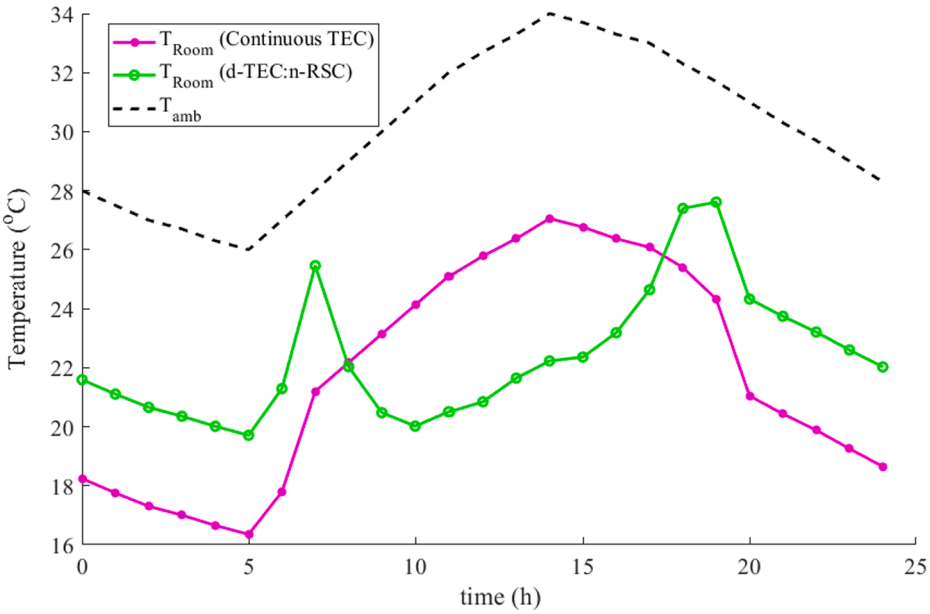

Fig. 13. Variation of the ambient and room temperatures throughout the day under the two modes of operation.

Factoring the battery's round trip efficiency would require even bigger PV and TEC sizes while the battery may need to be at least 5 kWh in size. Although 5 kWh lithium-ion battery products do exist, the investment will be very costly, thus these observations further support that the continuous TEC mode is overall not recommended. In contrast, as aforementioned in Section 5.1, the required thermal storage size to support the sunrise and sunset periods in the d-TEC:n-RSC mode can be 18.21 kg of paraffin, which is a significantly cheaper option, thus making this mode of operation a more practical option.

Based on Eqs. (10) and considering the cooling curve shown in Fig. 7 (b) for the d-TEC:n-RSC mode, it is found that the equivalent solar to cooling COP for the TEC and the total cooling power cases are 0.1099 and 0.2054, respectively. These numbers imply that the PV-TEC system's cooling power can be almost doubled if the RSC effect is integrated into it. Unfortunately, the value 0.2054 is still inferior to that of the PV-VCC implementation (reported as 1.85–2.25 by Salilih and Birhane [9]), which occurred most likely because the TEC naturally has a lower energy performance. On the bright side, as demonstrated by several previous studies [17,18], the PV-TEC system implementation is structurally simple over the PV-VCC system as it does not require working fluids and compressor components. Adding the RSC is also not expected to significantly increase the system complexity since the cooling energy is sourced from the same PV panel, so the proposed PV-RSC-TEC system may be an economical option for smaller building rooms. Indeed, conducting a techno-economic analysis and life cycle assessment would be a valuable future work to assess the feasibility of the PV-RSC-TEC system from the economic cost and greenhouse gas emission perspectives.

Meanwhile, the above analysis was based on real weather data and it has shown that the system performance is sensitive to many working parameters. Here, the effects of some key parameters are briefly summarized as follows:

1. TEC's COP is maximal when the hot side temperature T_H ideally equals T_{amb}, so cooling methods that can further reduce T_H towards T_{amb} while not consuming little energy is desirable. Indeed, active cooling methods generally require energy so this factor should be monitored in the design process.
2. A lower target T_{room} would indeed increase the cooling demand of the proposed system. Based on the results in Fig. 13 (b), the target T_{room} minimum stagnation point is very close to 20 °C, and a more powerful cooling technology such as the PV-VCC system may be preferred for lower temperatures. However, it should be noted that no attempt has been made to optimize the TEC module choice and that better options could enable an equivalent solar to cooling COP of up to 0.23 (after factoring in the 20% PV efficiency) [15].
3. Increasing the solar cell's power conversion efficiency and the TEC's COP would indeed be desirable factors to linearly increase the cooling power output and subsequently decrease the system sizing. Furthermore, increasing the building's wall thicknesses or choosing materials with lower thermal conductivities are alternative ways to decrease the cooling demand.
4. While a larger q_s will provide additional solar power and subsequently larger amounts of cooling power, generally days with higher average q_s will also increase T_{amb} and hence the cooling demand. It is projected that a certain q_s and subsequently T_{amb} condition will exist such that the required PV area $A_{PV(req)}$ will be minimum, a factor of which can be studied in future works. Meanwhile, a high RH environment has little effect on the PV-TEC cooling energy, but it will greatly degrade the RSC cooling power, so this system is more suitable in dryer climates.
5. It is noted that the current study is simulation-based and that certain factors will need to be additionally considered when developing an experimental platform or real implementation of the proposed system. These include I. The addition of airflow valves or "switches" required to change the airflow source and origin across the bottom of the PV panel during the day and night times; II. The addition of air blowers and their energy consumptions; III. The power electronic subsystems and wiring are needed to manage the power flows between the PV panel, TEC, battery, and auxiliary equipment. Although this may seem complex, it is noted that, in the conventional PV-VCC system, the same air blowers and power electronic subsystems would still be required. There, the power subsystem would be even more complex because it would need to convert DC power into the required AC power.

6. Conclusion

This paper has integrated the radiative sky cooling (RSC) ability of the PV cell to the PV-TEC system, which further increased the total cooling power output (and hence the energy utilization efficiency). A spectral model that involves the PV panel's emissivity spectrum is used to analyze the RSC ability, which is then coupled to the TEC model. The

overall PV-RSC-TEC system is applied for space cooling of an occupied building by estimating the building's cooling loads and calculating the corresponding PV surface area requirement. Two modes of operation for the PV-TEC component have been selected for analysis under 7 days of operation with time-varying solar irradiances, ambient temperature, and ambient relative humidity. The key findings of this paper include:

1. The continuous TEC mode (involving a battery for nighttime TEC operation) will cause excessive amounts of nighttime cooling power while the daytime cooling power was often insufficient. This leads to an unideal PV surface area requirement to properly meet all the cooling demands.
2. In contrast, the all-day TEC and all-night RSC (d-TEC:n-RSC) mode enabled a much better matched cooling supply-demand ratio throughout most of the day, but weak spots existed at the sunrise and sunset period due to problems caused by low solar irradiance. Notably, this problem can be easily solved by adding a thermal storage material.
3. Overall, the RSC ability of the common crystalline solar cells can increase the PV-TEC's equivalent solar to cooling coefficient of performance (from 0.1099 to 0.2054), and as such is worthwhile integrating. The PV area requirement was in the range of 12–17 m^2, which is much smaller than the studied room space (24 m^2), and a consistent temperature drop of up to 10 °C was achievable.

Declaration of Competing Interest

The authors declare that they have no known competing financial interests or personal relationships that could have appeared to influence the work reported in this paper.

Acknowledgments

This research was sponsored by the National Natural Science Foundation of China (NSFC 5171101721, NSFC 51776193) and the Fundamental Research Funds for the Central Universities (No. WK2090000021).

References

[1] E. Ramblings, The demand for cooling in Singapore's buildings, 2020/4/25; Available from: http://www.energyramblings.com/2015/09/05/the-demand-for-cooling-in-singapores-buildings/.
[2] Kharagpur, Vapour Compression Refrigeration Systems. 2020/2/27; Available from: https://nptel.ac.in/content/storage2/courses/112105129/pdf/RAC%20Lecture%2014.pdf.
[3] X. She, L. Cong, B. Nie, G. Leng, H. Peng, Y.i. Chen, X. Zhang, T. Wen, H. Yang, Y. Luo, Energy-efficient and -economic technologies for air conditioning with vapor compression refrigeration: A comprehensive review, Appl. Energy 232 (2018) 157–186.
[4] D.i. Liu, Y. Cai, F.-Y. Zhao, Optimal design of thermoelectric cooling system integrated heat pipes for electric devices, Energy 128 (2017) 403–413.
[5] D. Zhao, G. Tan, A review of thermoelectric cooling: Materials, modeling and applications, Appl. Therm. Eng. 66 (1-2) (2014) 15–24.
[6] M. Gong, G. Wall, Life Cycle Exergy Analysis of Solar Energy Systems, J. Fundament. Renew. Energy Appl. 5 (1) (2014).
[7] N.I. Ibrahim, F.A. Al-Sulaiman, F.N. Ani, Performance characteristics of a solar driven lithium bromide-water absorption chiller integrated with absorption energy storage, Energy Convers. Manage. 150 (2017) 188–200.
[8] N.I. Ibrahim, F.A. Al-Sulaiman, A. Saat, S. Rehman, F.N. Ani, Charging and discharging characteristics of absorption energy storage integrated with a solar driven double-effect absorption chiller for air conditioning applications, J. Storage Mater. 29 (2020) 101374, https://doi.org/10.1016/j.est.2020.101374.
[9] E.M. Salilih, Y.T. Birhane, Modelling and performance analysis of directly coupled vapor compression solar refrigeration system, Sol. Energy 190 (2019) 228–238.
[10] K.F. Fong, C.K. Lee, T.T. Chow, Improvement of solar-electric compression refrigeration system through ejector-assisted vapour compression chiller for space conditioning in subtropical climate, Energy Build. 43 (12) (2011) 3383–3390.
[11] S. Lu, R. Liang, J. Zhang, C. Zhou, Performance improvement of solar photovoltaic/thermal heat pump system in winter by employing vapor injection cycle, Appl. Therm. Eng. 155 (2019) 135–146.
[12] T.H. Kwan, Q. Yao, Thermodynamic and transient analysis of the hybrid concentrated photovoltaic panel and vapour compression cycle thermal system for combined heat and power applications, Energy Convers. Manage. 185 (2019) 232–247.
[13] N. Dimri, A. Tiwari, G.N. Tiwari, Effect of thermoelectric cooler (TEC) integrated at the base of opaque photovoltaic (PV) module to enhance an overall electrical efficiency, Sol. Energy 166 (2018) 159–170.
[14] R. Daghigh, Y. Khaledian, Effective design, theoretical and experimental assessment of a solar thermoelectric cooling-heating system, Sol. Energy 162 (2018) 561–572.
[15] K. Irshad, K. Habib, F. Basrawi, B.B. Saha, Study of a thermoelectric air duct system assisted by photovoltaic wall for space cooling in tropical climate, Energy 119 (2017) 504–522.
[16] K. Irshad, K. Habib, S. Algarni, B.B. Saha, B. Jamil, Sizing and life-cycle assessment of building integrated thermoelectric air cooling and photovoltaic wall system, Appl. Therm. Eng. 154 (2019) 302–314.
[17] K. Irshad, K. Habib, F. Basrawi, N. Thirumalaiswamy, R. Saidur, B.B. Saha, Thermal comfort study of a building equipped with thermoelectric air duct system for tropical climate, Appl. Therm. Eng. 91 (2015) 1141–1155.
[18] K. Irshad, K. Habib, N. Thirumalaiswamy, B.B. Saha, Performance analysis of a thermoelectric air duct system for energy-efficient buildings, Energy 91 (2015) 1009–1017.
[19] R. Basnet, et al., Impact of pre-fabrication treatments on n-type UMG wafers for 21% efficient silicon heterojunction solar cells, Sol. Energy Mater. Sol. Cells 205 (2020), 110287.
[20] H. Liao, Q. Deng, Y. Shen, G. Wang, S. Wang, Y. Mao, Theoretical analysis of doping concentration, layer thickness and barrier height effects on BaSi2 based homojunction solar cells toward high efficiency, Sol. Energy 201 (2020) 857–865.
[21] B. Zhao, M. Hu, X. Ao, G. Pei, Performance evaluation of daytime radiative cooling under different clear sky conditions, Appl. Therm. Eng. 155 (2019) 660–666.
[22] D. Zhao, A. Aili, Y. Zhai, S. Xu, G. Tan, X. Yin, R. Yang, *Radiative sky cooling: Fundamental principles, materials, and applications*, Appl. Phys. Rev. 6 (2) (2019) 021306, https://doi.org/10.1063/1.5087281.
[23] M. Zeyghami, D.Y. Goswami, E. Stefanakos, A review of clear sky radiative cooling developments and applications in renewable power systems and passive building cooling, Sol. Energy Mater. Sol. Cells 178 (2018) 115–128.
[24] P. Yang, C. Chen, Z.M. Zhang, A dual-layer structure with record-high solar reflectance for daytime radiative cooling, Sol. Energy 169 (2018) 316–324.
[25] S.Y. Jeong, C.Y. Tso, J. Ha, Y.M. Wong, C.Y.H. Chao, B. Huang, H. Qiu, Field investigation of a photonic multi-layered TiO2 passive radiative cooler in sub-tropical climate, Renewable Energy 146 (2020) 44–55.
[26] R.Y.M. Wong, C.Y. Tso, C.Y.H. Chao, B. Huang, M.P. Wan, Ultra-broadband asymmetric transmission metallic gratings for subtropical passive daytime radiative cooling, Sol. Energy Mater. Sol. Cells 186 (2018) 330–339.
[27] M. Muselli, Passive cooling for air-conditioning energy savings with new radiative low-cost coatings, Energy Build. 42 (6) (2010) 945–954.
[28] K. Zhang, D. Zhao, X. Yin, R. Yang, G. Tan, Energy saving and economic analysis of a new hybrid radiative cooling system for single-family houses in the USA, Appl. Energy 224 (2018) 371–381.
[29] B. Zhao, M. Hu, X. Ao, N. Chen, G. Pei, Radiative cooling: A review of fundamentals, materials, applications, and prospects, Appl. Energy 236 (2019) 489–513.
[30] A. Riverola, A. Mellor, D. Alonso Alvarez, L. Ferre Llin, I. Guarracino, C. N. Markides, D.J. Paul, D. Chemisana, N. Ekins-Daukes, Mid-infrared emissivity of crystalline silicon solar cells, Sol. Energy Mater. Sol. Cells 174 (2018) 607–615.
[31] D. Sato, N. Yamada, Review of photovoltaic module cooling methods and performance evaluation of the radiative cooling method, Renew. Sustain. Energy Rev. 104 (2019) 151–166.
[32] B. Zhao, M. Hu, X. Ao, N. Chen, Q. Xuan, Y. Su, G. Pei, A novel strategy for a building-integrated diurnal photovoltaic and all-day radiative cooling system, Energy 183 (2019) 892–900.
[33] H. Zhang, J. Yang, H. Wu, P. Fu, Y. Liu, W. Yang, Dynamic thermal performance of ultra-light and thermal-insulative aerogel foamed concrete for building energy efficiency, Sol. Energy 204 (2020) 569–576.
[34] U. Berardi, C. Sprengard, An overview of and introduction to current researches on super insulating materials for high-performance buildings, Energy Build. 214 (2020), 109890.
[35] K. Teffah, Y. Zhang, Modeling and experimental research of hybrid PV-thermoelectric system for high concentrated solar energy conversion, Sol. Energy 157 (2017) 10–19.
[36] Q. Wan, Y.-K. Teh, Y. Gao, P.K.T. Mok, Analysis and Design of a Thermoelectric Energy Harvesting System With Reconfigurable Array of Thermoelectric Generators for IoT Applications, IEEE Trans. Circuits Syst. I Regul. Pap. 64 (9) (2017) 2346–2358.
[37] J.J. Sanchez, W.H. Giedt, Thin films for reducing tamping gas convection heat transfer effects in a nif hohlraum, Fusion Technol. (2002).
[38] İ. Ceylan, et al., Determination of the heat transfer coefficient of PV panels, Energy 175 (2019) 978–985.
[39] T.H. Kwan, et al., Performance analysis of the sky radiative and thermoelectric hybrid cooling system, Energy 200 (2020) 117516, https://doi.org/10.1016/j.energy.2020.117516.
[40] A. Hajare, E. Elwakil, Integration of life cycle cost analysis and energy simulation for building energy-efficient strategies assessment, Sustainable Cities Soc. 61 (2020), 102293.
[41] PhysLink. How much heat per hour do humans dissipate?; Available from: https://www.physlink.com/education/askexperts/ae420.cfm.

[42] Sunpower. 430–450 W Commercial A-Series Panels. Available from: https://us.sunpower.com/sites/default/files/sp-a450-440-430-com-pv4s-gen42-ds-en-ltr-532726.pdf.
[43] P. Modules, Peltier Thermoelectric Cooling Modules. Available from: https://peltiermodules.com/peltier.datasheet/Peltier_Modules.pdf.
[44] D. Energy, What Is The Right Temperature For My Air Conditioner In Summer?; Available from: https://blog.directenergy.com/right-temperature-air-conditioner-summer/.
[45] Miqdam T. Chaichan, S.H.K. Abdul-Mohsen, N.M. Al-Ajeely, Thermal Conductivity Enhancement by using Nano-material in Phase Change Material for Latent Heat Thermal Energy Storage Systems, Saussurea 5 (6) (2015) 48–55.